TELKOMNIKA Telecommunication Computing Electronics and Control
Vol. 24, No. 1, February 2026, pp. 329~342
ISSN: 1693-6930, DOI: 10.12928/TELKOMNIKA.v24i1.27459

Improved disturbance rejection of induction motor drives using PI–VGSTASM control and torque disturbance estimation

Ngoc Thuy Pham, Duc Thuan Le, Thanh Tinh Pham
Department of Electrical Engineering Technology, Industrial University of Ho Chi Minh City, Ho Chi Minh, Vietnam

Article Info

Article history:

Received Aug 7, 2025
Revised Nov 26, 2025
Accepted Dec 8, 2025

Keywords:

Field-oriented control
Induction motor
Particle swarm optimization
Second-order sliding mode disturbance rejection
Super-twisting algorithm torque estimation
Variable-gain super-twisting algorithm

ABSTRACT

Induction motor (IM) drives often suffer performance degradation under load variations and parameter uncertainties when using conventional proportional–integral (PI)- based field-oriented control (FOC). To address these issues, this study proposes a composite control framework combining a PI regulator in the speed loop with a Lyapunov-based variable-gain super-twisting algorithm (VGSTA) for the inner current loops to enhance robustness against disturbances and parameter variations. In addition, a load torque observer is developed to estimate unknown disturbances in real time and generate an equivalent compensation current, thereby improving disturbance rejection. Unlike existing approaches, the proposed strategy achieves a balance between simplicity, robustness, and smooth control by integrating classical PI control with higher-order sliding mode techniques and adaptive observer dynamics. Furthermore, the controller and observer gains are optimized using particle swarm optimization (PSO) to improve convergence and reduce overshoot under uncertain conditions. Simulation results demonstrate accurate speed regulation, effective chattering reduction, and reliable operation under load and parameter variations. Due to its low computational complexity and high robustness, the proposed method is well suited for industrial drive systems and electric mobility applications.

Corresponding Author:

Ngoc Thuy Pham
Department of Electrical Engineering Technology, Industrial University of Ho Chi Minh City
12 Nguyen Van Bao street, Hanh Thong ward, 700000 Ho Chi Minh, Vietnam
Email: Ngocpham1020@gmail.com

1. INTRODUCTION

The three-phase induction motor (IM) has long been recognized as the workhorse of the modern industry, owing to its simple construction, high reliability, low cost, and robust operational capabilities, even in the most demanding environments [1], [2]. From domestic applications such as pumps and fans to complex industrial systems like steel mills, elevators, and, more recently, electric vehicles, the presence of the induction motor is indispensable [3], [4]. However, the inherent nature of the IM is that of a nonlinear, multi-input-multi-output (MIMO) system with parameters that vary with operating conditions, making its high-performance control a significant scientific challenge [5], [6].

To unlock the full potential of the induction motor, the field-oriented control (FOC) methodology was developed and has since become the gold standard for high-performance drives [7], [8]. The core principle of FOC is to transform the dynamic model of the IM from the stationary $\alpha\beta$ reference frame to a synchronous dq reference frame, thereby decoupling the stator current components. The direct-axis current component (id) is used to control the rotor flux, while the quadrature-axis current component (iq) controls the electromagnetic torque. This decoupling effectively makes the IM behave like a separately excited direct current (DC) motor, enabling fast torque response and precise speed control [9], [10]. The conventional FOC

structure typically employs a cascaded arrangement of linear proportional-integral (PI) controllers: one for the outer speed loop and two for the inner id and iq current loops [11].

Despite its proven effectiveness and widespread application due to design simplicity, this classic PI-PI structure reveals inherent limitations when faced with the increasingly stringent demands of modern applications [12], [13]. Firstly, PI controllers are linear and are tuned for optimal performance at a specific operating point. Consequently, their control quality degrades significantly when the system is subjected to load variations, parameter uncertainties, and unmodeled external disturbances [14]. Secondly, a major challenge in indirect FOC is its strong dependency on the accuracy of motor parameters, especially the rotor time constant ($Tr = Lr/Rr$). The rotor resistance (Rr) can vary by up to 100% of its nominal value due to thermal effects, causing errors in the slip frequency calculation and leading to an inaccurate field orientation [15], [16]. This detuning results in performance degradation, increased power losses, and can even lead to system instability [17], [18]. Thirdly, the outer speed loop with its PI controller has a limited bandwidth, leading to a sluggish response to sudden load torque changes [19]. This causes undesirable speed drops and prolonged recovery times, which are unacceptable in applications requiring high dynamic stiffness, such as computer numerical control (CNC) machine tools and industrial robotics [20], [21].

To address the aforementioned challenges, the research community has proposed numerous advanced control strategies. Nonlinear techniques such as sliding mode control (SMC), backstepping control, neural network have been applied to replace PI controllers for enhanced robustness [22]-[24]. Among these, SMC is distinguished by its absolute robustness to matched uncertainties and disturbances. However, conventional first-order SMC suffers from the detrimental chattering phenomenon, which can induce torque ripples and excite undesired mechanical resonances [25]-[28]. To overcome this issue, second-order sliding mode (SOSM) controllers, such as the super-twisting algorithm, variable-gain super-twisting algorithm (VGSTA) have emerged as a superior solution, effectively eliminating chattering while preserving the excellent robustness properties of SMC [29]-[34]. Furthermore, hybrid control strategies also have attracted considerable attention, as their integrated structure enables the exploitation of the strengths of different control approaches while mitigating their inherent limitations, thereby improving the dynamic performance and overall efficiency of drive systems [35]-[39]. In parallel, to tackle the problem of load disturbances, disturbance observers (DOB) have been developed to actively estimate and compensate for these external effects. These observers act as a feedforward channel, significantly improving the system's disturbance rejection capability without affecting the stability of the closed loop [40], [41].

Motivated by the foregoing analysis, this paper proposes a robust hybrid control structure for an induction motor drive using PI-VGSTASM control and torque disturbance estimation (PI VGSTASM TE) to simultaneously achieve fast dynamic response and superior disturbance rejection capabilities. The proposed structure comprises: (i) a conventional PI controller for the outer speed loop to ensure zero steady-state error and straightforward tuning ; (ii) SOSM controllers based on VGSTA for the inner id and iq current loops, designed to achieve fast, precise current response while completely eliminating chattering; and (iii) the cornerstone of this research, the design of a nonlinear disturbance observer to accurately estimate the "torque disturbance," which includes the external load torque and other system uncertainties. This estimated value is fed forward to the isq reference command, creating a proactive and rapid disturbance compensation mechanism. To ensure robust and high-performance control for both the disturbance observer and the controller for in the inner current loops which using the VGSTA require appropriate tuning of several key parameters. Manual tuning of these parameters is time-consuming and may lead to suboptimal performance, particularly under nonlinear operating conditions of the induction motor drives (IMDs) [42], [43]. To overcome this limitation, particle swarm optimization (PSO) was adopted as an offline global search technique.

The main contributions of this paper are summarized as follows: i) proposing a hybrid control structure that synergistically combines PI, VGSTASM, and a torque disturbance observer; ii) a detailed VGSTASM-based current controller, which enhances the transient response and robustness of the inner control loop without inducing chattering; iii) developing an effective disturbance observer based on VGSTASM and integrating it into the control architecture as a feedforward compensation channel, thereby significantly improving the dynamic stiffness and load disturbance rejection capability of the drive; and iv) using PSO as an offline global search technique for the parameters of observer and control. The remainder of this paper is organized as follows. Section 2 presents the mathematical model of the induction motor and the principles of field-oriented control (FOC) and details the design of the proposed control structure, including the PI speed controller, the VGSTASM current controllers, and the disturbance observer. Section 3 presents the simulation and experimental results. Finally, section 4 provides the conclusions of this research.

2. METHOD

2.1. Model of induction motor drives

In this study, the FOC technique recognized as the dominant approach in industrial motor drive applications is employed [1]. When the rotor flux is perfectly aligned with the d-axis, the quadrature-axis flux component becomes zero, allowing the current components i_{sd}; i_{sq} to independently regulate the rotor flux and the electromagnetic torque. The dynamic behavior of the induction motor can then be expressed by the following space-vector differential equations:

$$\begin{cases} \dfrac{d\omega_r}{dt} = \dfrac{3}{2}P\dfrac{\delta\sigma L_S}{J}(\psi_{rd}i_{sq}) - \dfrac{T_L}{J} - B'_{\omega_r} \\ \dfrac{d\psi_{rd}}{dt} = \dfrac{L_m}{\tau_r}i_{sd} - \dfrac{1}{\tau_r}\psi_{rd} \\ L_S\dfrac{di_{sq}}{dt} = -ai_{sq} + L_s\omega_e i_{sd} + b_r\omega_e\psi_{rd} + cu_{sq} \\ L_S\dfrac{di_{sd}}{dt} = -ai_{sd} + L_s\omega_e i_{sq} + bR_r\psi_{rd} + cu_{sd} \end{cases} \quad (1)$$

where: $\sigma = 1 - \frac{L_m^2}{L_S L_r}; \delta = \frac{L_m}{\sigma L_S L_r}; a = \frac{L_m^2 R_r + L_r^2 R_s}{\sigma L_r^2}; b = \frac{L_m^2 R_r}{\sigma L_r^2}; c = \frac{1}{\sigma}; \tau_r = \frac{L_r}{R_r}; bB' = \frac{B}{J}$

u_{sd}; u_{sq}; i_{sd}; i_{sq}: the components of stator voltage and stator current, respectively, ψ_{rd}, ψ_{rq}: rotor flux components; T_e, T_L: electromagnetic and load torque; $d-q$; $D-Q$: synchronous and stationary axis reference frame quantities, respectively; ω_r: the angular velocity (mechanical speed), $\omega_r = (2/P)\omega_{re}$; ω_{re}, ω_{sl}, ω_e: the electrical speed respectively rotor and slip angular and synchronous angular velocity; L_s, L_r: stator and rotor inductances; L_m: mutual inductance; R_s, R_r: stator and rotor resistances; J: the inertia of motor and load; σ: total linkage coefficient; P: number of pole pairs; B: friction coefficient; τ_r: rotor and stator time constant. The electromagnetic torque and the slip frequency can be expressed in dq reference frame:

$$T_e = \frac{3P}{2}\frac{L_m}{L_r}\psi_{rd}i_{sq} \quad (2)$$

$$\omega_{sl} = \frac{M}{L_r}\psi_{rd}i_{sq} \quad (3)$$

2.2. Speed proportional–integral controller design

In the outer-loop of the FOC structure, a PI controller is adopted to regulate the rotor speed of the IM. The PI controller generates a torque-producing current reference i_q^* based on the speed tracking error $e_\omega = \omega_r^* - \omega_r$, where ω_r^*, ω_r are the reference and actual rotor speeds, respectively. The PI speed controller is given by:

$$C(s) = K_{ps} + \frac{K_{is}}{s} \quad (4)$$

The mechanical dynamics of the induction motor are modeled as:

$$G(s) = \frac{K_t}{\tau_m s+1} \quad (5)$$

where: K_t is the torque constant, $\tau_m = J/B$ is the mechanical time constant, J is the rotor inertia, B is the viscous friction coefficient.

The closed-loop transfer function of the speed control loop is then derived as:

$$\frac{\omega_r^*(s)}{\omega_r(s)} = \frac{\left(K_{ps}+\frac{K_{is}}{s}\right)\cdot\left(\frac{K_t}{\tau_m s+1}\right)}{1+\left(K_{ps}+\frac{K_{is}}{s}\right)\cdot\left(\frac{K_t}{\tau_m s+1}\right)} \quad (6)$$

To design the PI gains, the denominator of (9) is equated with the standard second-order system:

$$s^2 + 2\zeta\omega_n s + \omega_n^2 \tag{7}$$

Comparing the coefficients yields:

$$2\zeta\omega_n = \frac{K_t K_{ps}}{\tau_m} + \frac{1}{\tau_m} \tag{8}$$

$$\omega_n^2 = \frac{K_t K_{is}}{\tau_m} \tag{9}$$

By selecting the desired damping ratio ζ / zeta and natural frequency ω_n / omega_n, the PI parameters can be computed as:

$$K_{ps} = \frac{2\zeta\omega_n\tau_m - 1}{K_t}, \quad K_{is} = \frac{\omega_n^2\tau_m}{K_t} \tag{10}$$

Typically, ζ=0.707 = 0.707 is chosen to ensure a critically damped response, and ω_n is selected according to the required speed loop bandwidth. A block diagram of the speed control loop is shown in Figure 1.

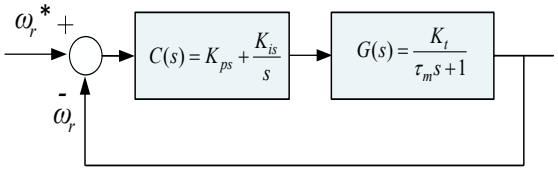

Figure 1. A block diagram of the speed control loop

2.3. SMC design with the VGSTA for in the inner current loops

In this part, a high-order nonlinear sliding control algorithm based on Lyapunov stability theory using the VGSTA is proposed for the inner current loops to increase robustness of overall system, minimizing the effects of parameter variations and unforeseen disturbances in the control process. The current error tracking function defined:

$$\varepsilon_{isd} = i_{sd}^* - i_{sd};\ \varepsilon_{isq} = i_{sq}^* - i_{sq} \tag{11}$$

The corresponding nonlinear slip surface according to the current components is defined as follows [44], [45]:

$$\begin{cases} S_1 = \varepsilon_{\mathrm{isd}} + k_1 \left| \int \varepsilon_{\mathrm{isd}} dt \right|^{1/2} sat(\int \varepsilon_{\mathrm{isd}} dt) \\ S_2 = \varepsilon_{\mathrm{isq}} + k_2 \left| \int \varepsilon_{\mathrm{isq}} dt \right|^{1/2} sat\left(\int \varepsilon_{\mathrm{isq}} dt\right) \end{cases} \tag{12}$$

Combining (1), taking the time differential on both sides of (12), we get:

$$\frac{dS_1}{dt} = \frac{d\varepsilon_{\mathrm{isd}}}{dt} + \frac{d}{dt}\left[k_1 \left| \int \varepsilon_{\mathrm{isd}} dt \right|^{1/2} sat(\int \varepsilon_{\mathrm{isd}} dt)\right]$$

$$\frac{di_{sd}^*}{dt} - \frac{1}{L_s}\left[-\mathrm{ai_{sd}} + \mathrm{L_s}\omega_e i_{\mathrm{sq}} + \mathrm{bR}_r\psi_{\mathrm{rd}} + \mathrm{cu_{sd}}\right] + \frac{d}{dt}\left[k_1 \left| \int \varepsilon_{\mathrm{isd}} dt \right|^{1/2} sat(\int \varepsilon_{\mathrm{isd}} dt)\right] = -v_1$$

$$\frac{dS_2}{dt} = \varepsilon_{\mathrm{isq}} + k_2 \left| \int \varepsilon_{\mathrm{isq}} dt \right|^{1/2} sat\left(\int \varepsilon_{\mathrm{isq}} dt\right)$$

$$= \frac{di_{sq}^*}{dt} - \frac{1}{L_s}\left[-\mathrm{ai_{sq}} - \mathrm{L_s}\omega_e i_{\mathrm{sd}} - \mathrm{b}_r\omega_e\psi_{\mathrm{rd}} + \mathrm{cu_{sq}}\right] + \frac{d}{dt}\left[k_2 \left| \int \varepsilon_{\mathrm{isq}} dt \right|^{1/2} sat\left(\int \varepsilon_{\mathrm{isq}} dt\right)\right] = -v_2 \tag{13}$$

In this proposed we select the v_1, v_2 switching control functions:

$$\begin{cases} v_1(t) = k_{\alpha 1}(t, \varepsilon_{\mathrm{isd}}) \left[\delta_1 \phi_1(S_1) + \mu_1 \int_0^t \phi_2(S_1) dt\right] \\ v_2(t) = k_{\alpha 2}(t, \varepsilon_{\mathrm{isq}}) \left[\delta_2 \phi_1(S_2) + \mu_2 \int_0^t \phi_2(S_2) dt\right] \end{cases} \quad (14)$$

where:

$$k_{\alpha 1}(t, \varepsilon_{\mathrm{isd}}) = S_1 sat(S_1); k_{\alpha 2}(t, \varepsilon_{\mathrm{isq}}) = S_2 sat(S_2)$$

$$\phi_1(S_x) = |S_x|^{1/2} sat(S_x) + k_3 S_x;\ \phi_2(S_x) = \frac{1}{2} sat(S_x) + \frac{3}{2} k_3 |S_x|^{1/2} sat(S_x) + k_3^2 S_x$$

With x = 1:2, $k1$, $k2$, $k3$, $\delta 1$, $\delta 2$, $\mu 1$, $\mu 2$ are positive coefficients. From (13)-(14) the virtual control functions of the current control loop are determined as follows:

$$\begin{cases} u_{sd}^* = \frac{L_s}{c}\left\{v_1(t) + \frac{di_{sd}^*}{dt} + \frac{d}{dt}\left[k_1 \left|\int \varepsilon_{\mathrm{isd}} dt\right|^{1/2} sat\left(\int \varepsilon_{\mathrm{isd}} dt\right)\right]\right\} + + \frac{1}{c}\left[\mathrm{ai_{sd}} - \mathrm{L}_s \omega_e i_{\mathrm{sq}} - \mathrm{bR}_r \psi_{\mathrm{rd}}\right] \\ u_{sq}^* = \frac{L_s}{c}\left\{v_2(t) + \frac{di_{sq}^*}{dt} + \frac{d}{dt}\left[k_2 \left|\int \varepsilon_{\mathrm{isq}} dt\right|^{1/2} sat\left(\int \varepsilon_{\mathrm{isq}} dt\right)\right]\right\} + + \frac{1}{c}\left[\mathrm{ai_{sq}} + \mathrm{L}_s \omega_e i_{\mathrm{sd}} + \mathrm{b}_r \omega_e \psi_{\mathrm{rd}}\right] \end{cases} \quad (15)$$

We select the Lyapunov function:

$$V = \frac{1}{2}[S_1^2 + S_2^2] \quad (16)$$

Differentiate both sides of (16), combine with formulas (13) and (14) to get:

$$\begin{aligned} &\frac{dV}{dt} = S_1 \frac{dS_1}{dt} + S_2 \frac{dS_2}{dt} \\ &= -k_{\alpha 1}(t, \varepsilon_{\mathrm{isd}}) S_1 \left[\phi_1(S_1) + \int_0^t \phi_2(S_1) dt\right] - k_{\alpha 2}(t, \varepsilon_{\mathrm{isq}}) S_2 \left[\phi_1(S_2) + \int_0^t \phi_2(S_2) dt\right] \end{aligned} \quad (17)$$

From (17), we see that the differential of the Lyapunov function is always negative. Therefore, the system is always stable.

2.4. Design of the adaptive VGSTASM disturbance observer

The dynamics of the IM are commonly described in the synchronous rotating reference frame ($d-q$ frame), under the FOC assumption, the electromagnetic torque T_e and the rotor speed ω are expressed as in (2). On the other hand, we also have:

$$J \cdot \frac{d\omega_r}{dt} = T_e - T_L - B \cdot \omega_r \quad (18)$$

where: ω_r is the mechanical rotor speed, J is the total moment of inertia of the motor and load, B is the viscous friction coefficient, T_L is the external load torque.

For control design, we can combine these equations. Let, $k_t = 3pL_m\psi_r/2L_r$ be the nominal torque constant. The (18) becomes:

$$\frac{d\omega_r}{dt} = \frac{k_t}{J} i_{sq} - \frac{B}{J}\omega_r - \frac{1}{J} T_L \quad (19)$$

where: i_{sq} is the q-axis stator current, which acts as the torque-producing current, p is the number of pole pairs, L_m, L_r are the mutual and rotor inductances, respectively, ψ_r is the constant rotor flux linkage.

2.4.1. Control problem formulation

The control objective is to design a controller for the q-axis current i_{sq} such that the rotor speed ω_r accurately tracks a desired reference speed ω_r^*, despite the presence of uncertainties and external disturbances. Let us define the state variables for the speed control loop as $x_1 = \omega_r^* - \omega_r^*$ (tracking error) and $x_2 = \dot{\omega}$. The system dynamics can be expressed in a simplified state-space form suitable for controller design:

$$\dot{x}_2(t) = \frac{k_t}{J} u + d(t) \quad (20)$$

where: $u = i_{sq}$ is the control input, (kt/J) are the nominal system parameters, $d(t)$ is the disturbance, defined as:

$$d(t) = -\frac{B}{J}\omega_r - \frac{1}{J}T_L + \Delta(t) \tag{21}$$

here, $\Delta(t)$ represents the effects of parameter variations ($\Delta k, \Delta J$) and unmodeled nonlinearities.

2.4.2. Design of the adaptive VGSTASM disturbance observer

This section presents the design of a novel direct adaptive higher-order sliding mode disturbance observer (OB). The observer's goal is to provide a high-precision, real-time estimation $\hat{d}(t)$ of the lumped disturbance $d(t)$. The lumped disturbance $d(t)$ is a continuously differentiable function, and its first time derivative $\dot{d}(t)$ is bounded by an unknown positive constant L, $|\dot{d}(t)| \leq L$. We design the observer to directly estimate $d(t)$. Let z is an internal state variable of the observer. Its dynamics are defined as:

$$\dot{z}(t) = \frac{k_t}{J}u + \hat{d} \tag{22}$$

where $\hat{d}$ is the estimated disturbance. A sliding variable s is defined using measurable and internal states:

$$s(t) = \omega_r(t) - z(t) \tag{23}$$

The derivative of the sliding variable s can be calculated by subtracting (22) from the time derivative of ω (which is x_2 from (20)):

$$\dot{s}(t) = \dot{\omega}_r - \dot{z} = \left(\frac{k_t}{J}u + d\right) - \left(\frac{k_t}{J}u + \hat{d}\right) \tag{24}$$

$$\dot{s}(t) = d - \hat{d} \tag{25}$$

Let $e_d = d - \hat{d}$ be the disturbance estimation error. The (25) shows that the derivative of our computable sliding variable s is exactly equal to the estimation error e_d. To drive the estimation error e_d to zero, we must first drive the sliding variable s to zero in finite time. We employ the VGSTA to achieve this, the derivative of $\dot{s}$:

$$\ddot{s}(t) = \dot{e}_d = \dot{d} - \dot{\hat{d}} \tag{26}$$

We design the law for $\hat{d}$ to be an adaptive VGSTA that counteracts the unknown perturbation $d(t)$:

$$\dot{\hat{d}}(t) = v_{GSTA}(t) \tag{27}$$

$$v_{GSTA}(t) = k_{\alpha 3}(t, \varepsilon_{\text{isd}})\left[\delta_3\phi_1\big(s(t)\big) + \mu_3\int_0^t \phi_2\big(s(t)\big)dt\right] \tag{28}$$

where:

$$\begin{cases} k_{\alpha 3}(t, \varepsilon_{\text{isd}}) = s(t)sat\big(s(t)\big) \\ \phi_1\big(s(t)\big) = |s(t)|^{1/2}sat\big(s(t)\big) + k_3 s(t) \\ \phi_2\big(s(t)\big) = \frac{1}{2}sat\big(s(t)\big) + \frac{3}{2}k_3|s(t)|^{1/2}sat\big(s(t)\big) + k_3^2 s(t) \end{cases}$$

From (19)-(21), the disturbance compensation current i_{sq}^{dis} can be computed as:

$$i_{sq}^{dis} = \frac{J}{k_t}\big(\dot{\omega} - \hat{d}\big) \tag{29}$$

Accordingly, the total reference current is given by:

$$i_{sq}^{ref} = i_{sq}^{*} + i_{sq}^{dis} \tag{30}$$

2.4.3. Adaptive laws and stability analysis

The key innovation is the design of the adaptive laws for $\lambda_1(t)$ and $\lambda_2(t)$ to eliminate the need for knowing the bound L. We propose the "increase-when-needed" adaptive laws:

$$\dot{\lambda}_1(t) = \begin{cases} k_1 \cdot |s|, & \text{if } |s| > \varepsilon_0 \\ -k_2 \cdot \lambda_1(t), & \text{if } |s| \le \varepsilon_0 \end{cases} \quad (31)$$

$$\dot{\lambda}_2(t) = \begin{cases} k_3 \cdot |s|, & \text{if } |s| > \varepsilon_0 \\ -k_4 \cdot \lambda_2(t), & \text{if } |s| \le \varepsilon_0 \end{cases} \quad (32)$$

where: s is the sliding variable defined in (23), k_1, k_2, k_3, k_4 are positive design constants that determine the adaptation rates, ε_0 is a small positive constant defining the width of the boundary layer around the sliding surface $s = 0$. It should be emphasized that the adaptive gains $\lambda 1(t)$ and $\lambda 2(t)$ are not constant values, but are dynamically updated online according to (31) and (32). In practice, at each time instant, the values of $\lambda 1(t)$ and $\lambda 2(t)$ are obtained by integrating their respective differential equations. When the sliding variable s is larger than the threshold ε_0, the gains increase proportionally to $|\ s\ |$, which enhances the disturbance rejection capability. Conversely, when $|\ s\ |$ falls below ε_0, the gains decay exponentially, thus preventing unnecessarily large values and reducing chattering. This "increase-when-needed" mechanism eliminates the need for prior knowledge of the disturbance bound L, while ensuring finite-time convergence and robustness of the adaptive VGSTA.

The stability of the complete adaptive observer system, described by (24)–(28), can be rigorously established using Lyapunov theory. The analysis shows that all error signals and adaptive gains remain uniformly ultimately bounded (UUB). Consequently, the disturbance estimation error e_d converges to a small, user-defined neighborhood of the origin within finite time**.** Furthermore, the estimated output $\hat{d}(t)$, obtained through the integration in (27), provides a continuous and accurate approximation of the actual disturbance.

2.5. PSO-based optimization of controller gains

To ensure robust and high-performance control, the Adaptive VGSTASM disturbance observer and the VGSTA for in the inner current loops require appropriate tuning of several key parameters. Manual tuning of these parameters is time-consuming and may lead to suboptimal performance, particularly under nonlinear operating conditions of the IMDs. To overcome this limitation, PSO was adopted as an offline global search technique. The optimization objective was defined as a multi-criteria cost function:

$$f(t) = w_1 f_1(t) + w_2 f_2(t) + w_3 f_3(t) \quad (33)$$

where $f_1(t)$ represents the integral of squared speed error, $f_2(t)$ quantifies high-frequency oscillations of the control signal, and $f_3(t)$reflects the total energy of the control input. The weighting coefficients $w_1;\ w_2; w_3$ were selected according to the desired trade-off between tracking accuracy, smoothness, and energy efficiency. Standard PSO velocity and position updates were employed:

$$v_i^{k+1} = \rho v_i^k + c_1 r_1 \left(p_i - x_i^k\right) + c_2 r_2 \left(g - x_i^k\right)$$

$$x_i^{k+1} = x_i^k + v_i^{k+1} \quad (34)$$

where $\rho$is the inertia weight, $c_1;\ c_2$are cognitive and social learning coefficients, and p_i and g denote the personal and global best solutions. Constriction factors and velocity clamping were applied to ensure stability and convergence. The PSO adaptive function is chosen as follows:

$$J = \int_0^t |e(t)| dt \quad (35)$$

The swarm optimization algorithm is implemented as shown in Figure 2. The optimization process stopped when either the maximum iteration limit was reached or improvements over five consecutive iterations fell below a preset tolerance. The global best particle yielded the optimal offline parameters and sliding-mode gains, which were later used as initial values for online adaptation. By employing PSO as a global optimizer, the proposed scheme achieved a near-optimal starting point, ensuring fast convergence and strong performance consistency across various operating conditions.

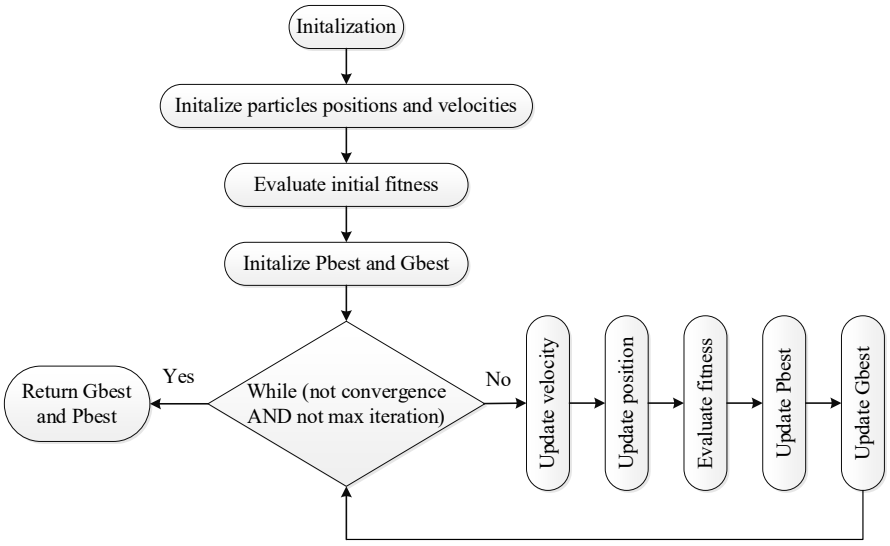

Figure 2. PSO algorithm flowchart

3. RESULTS AND DISCUSSION

To validate the effectiveness and superiority of the proposed control strategy, comprehensive simulations are conducted in the MATLAB/Simulink environment. The parameters ratings of the 1.5 kW induction motor used in the simulation are: 400 V, 50 Hz, 2 pole, 2880 rpm, Rs = 1.97 Ω, Rr = 1.96 Ω, Ls = 0.0154 H, Lr = 0.0154 H, Lm = 0.3585 H, J = 0.00242 kg.m2, B = 0.0005. The simulation model is presented in Figure 3. To evaluate performance, comparisons were made against the conventional PI, the PI–SOSM control strategy with a torque observer based on super-twisting algorithm (PI SOSM OB), and several advanced methods from the literature in [40]-[42], [44].

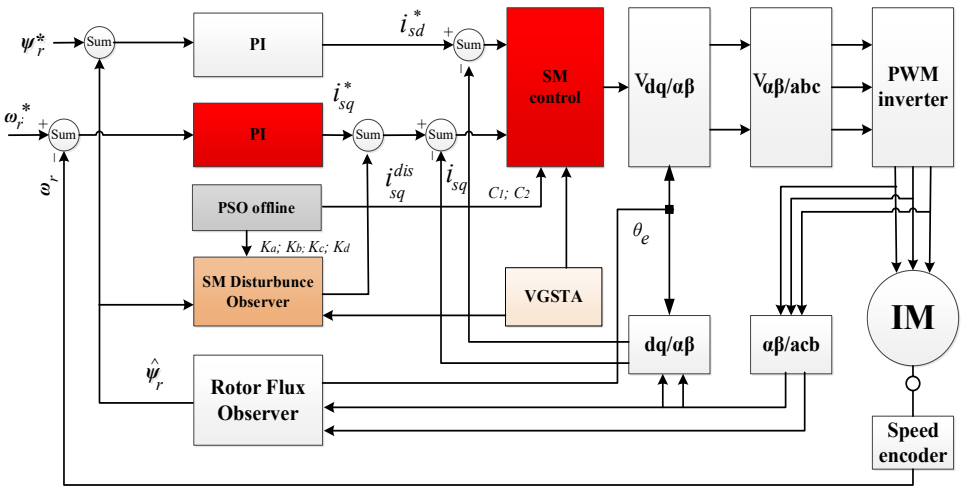

Figure 3. The vector control of IM drive using PI_VGSTA control

3.1. Tracking performance and load torque disturbance rejection

To evaluate the dynamic performance and disturbance rejection capability of the proposed control strategy, three controllers were comparatively tested under identical conditions: the conventional PI controller, the PI–SOSM OB, and the proposed PI–VGSTASM with torque estimation approach that based on VGSTASM. The reference speed varied between +315 rad/s, –315 rad/s, and 70 rad/s, including several reversal and load disturbance events with step load torque TL of 7 Nm is applied at t = 0.2 s and removed at t = 0.5.

Figure 4(a) shows the speed tracking performance of the three controllers. The PI scheme exhibits a slower transient response with a noticeable overshoot, while the PI–SOSM observer significantly improves rise time and suppresses oscillations. The proposed PI–VGSTASM TE demonstrates the fastest convergence to the reference speed, achieving a settling time of 0.0363 s, which is 11.5% shorter than that of the PI–SOSM OB and 17.7 % shorter than the basic PI control. Moreover, the overshoot is effectively minimized to 0.0114 rad/s, confirming the superior transient stability of the hybrid VGSTASM-based current loop. Figure 4(b) shown that, the torque of the PI controller exhibits relatively high ripple during sudden load changes, while the SOSM observer helps to reduce torque chattering. The VGSTASM-based estimation further smooths the torque response, maintaining stable torque compensation with minimal oscillation amplitude. This improvement results from the variable gain super-twisting algorithm's adaptive nature, which mitigates high-frequency disturbances without sacrificing response speed.

Figures 4(c) and (d) depict the instantaneous speed error and I_{sd} current, respectively. The PI–VGSTASM TE produces the smallest speed deviation, with near-zero steady-state error under both load and speed transients. Meanwhile, the current response of the proposed method remains smooth and well-regulated, demonstrating effective decoupling between torque and flux components. Table 1 summarizes the performance indices for the three control schemes. The proposed PI VGSTASM TE achieves the lowest integral of squared error (ISE) = 9.15×10^{-4}, integral of absolute error (IAE) = 0.0141, and root mean square error (RMSE)_speed = 0.0594, indicating remarkable precision and noise immunity.

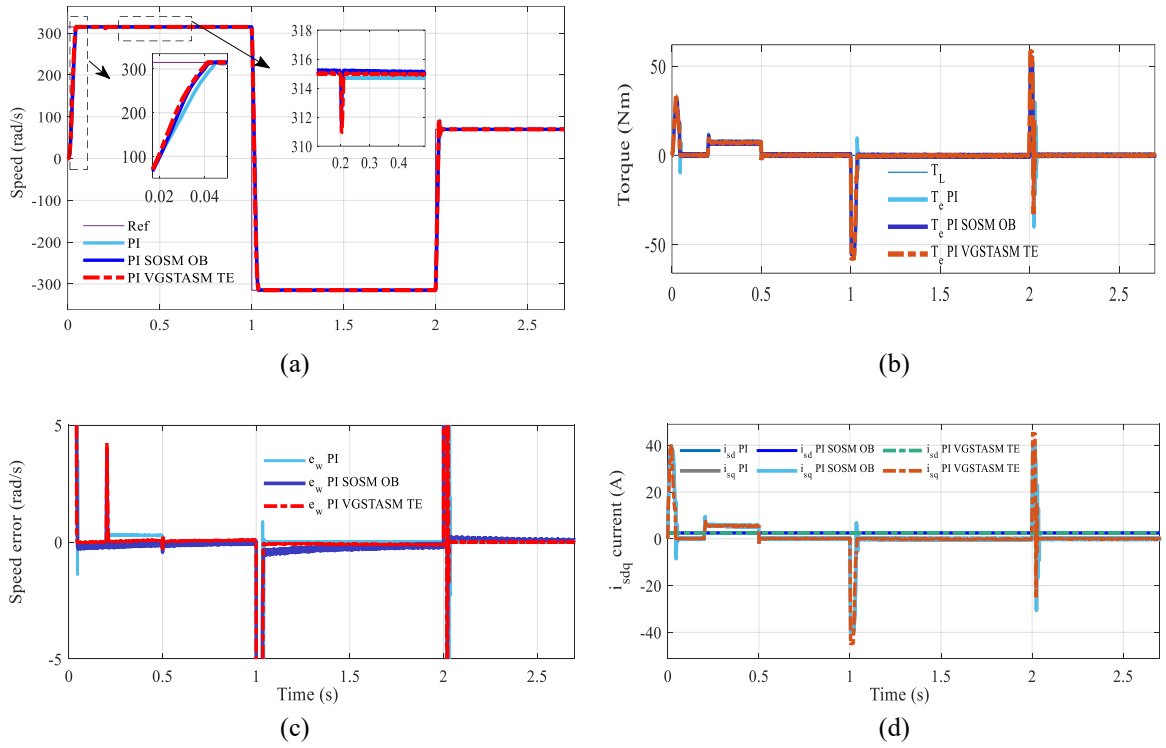

Figure 4. Comparative tracking and disturbance rejection and observer performance: (a) speed response for two controller strategy, (b) torque response, (c) speed tracking error, and (d) i_{sdq} current for three controllers

Table 1. Indices for evaluating control performance

Control strategy	Settling time	Overshoot	ISE	IAE	RMSE_speed
PI	0.0441	0.4407	0.0217	0.0751	0.2890
PI SOSM OB	0.0410	0.0934	0.0040	0.0282	0.1244
PI VGSTASM TE	0.0363	0.0114	9.1504e-4	0.0141	0.0594

Compared with the Fuzzy–PI method in [41], the approach fails to maintain stability during zero-crossing reversals, leading to transient irregularities. The hybrid STA–SMC with fuzzy logic compensation in [42] achieved fast recovery (4 ms) and negligible steady-state error, but residual speed and torque oscillations remained due to incomplete chattering suppression. The adaptive Fuzzy–PI in [44] improved zero-speed

transition smoothness but showed slower convergence and larger steady-state error under varying loads. Likewise, the nonlinear DTC with a super-twisting MRAS observer reduced speed drop (972 rad/s, ≈ 4.2%) and steady-state error (28 rad/s, ≈ 2.8%), yet introduced noticeable oscillations.

In contrast, the proposed PI–VGSTASM TE controller achieves the best overall performance, offering faster transients, minimal torque ripple, and smaller tracking errors. By integrating VGSTASM-based torque estimation into the current loop, it ensures both high accuracy and strong robustness against load disturbances ideal for high-performance induction motor drives.

3.2. Robustness test against parameter uncertainty

To verify the robustness of the proposed PI–VGSTASM TE controller, comparative simulations were conducted under two main parameter disturbances: (i) a 100% increase in the rotor resistance Rr and (ii) a 100% increase in the total moment of inertia J. In both cases, all control gains were kept constant at their nominal values.

3.2.1. Influence of rotor resistance variation

Figures 5(a) and (b) presents the speed and torque responses when the rotor resistance Rr is doubled. The conventional PI controller exhibits a significant degradation, characterized by oscillatory behavior and slower convergence to the reference speed. The PI–SOSM OB improves disturbance rejection through sliding action, but residual ripples and a slightly delayed transient remain evident. In contrast, the proposed PI–VGSTASM TE structure demonstrates superior resilience, maintaining smooth torque and stable speed tracking response without noticeable overshoot.

This improvement stems from the enhanced disturbance estimation capability of the VGSTASM observer, which models the variation of Rr as a lumped disturbance $d(t)$. By compensating this term in real time, the controller preserves fast convergence and stable dynamics, even under severe electrical parameter drift.

Further analysis at high operating speeds (280 rad/s) (Figure 5(a)), the variation in Rr has a much stronger influence to speed and torque. Under this condition, the PI control strategy show noticeable overshoot and oscillations. Meanwhile, the PI_SOSM OB and PI–VGSTASM TE controller maintains more stable operation. This robustness arises because the variation Rr in modeled as part of the disturbance $d(t)$, which is effectively estimated and compensated by disturbance observer, in particular, the PI–VGSTASM TE strategy demonstrates a superiority over the PI–SOSM OB because it employs the VGSTA algorithm for both the current controller and the disturbance observer, while all controller and observer coefficients are optimally tuned using the PSO algorithm. These enhancements significantly improve the disturbance rejection capability and overall robustness of the proposed method.

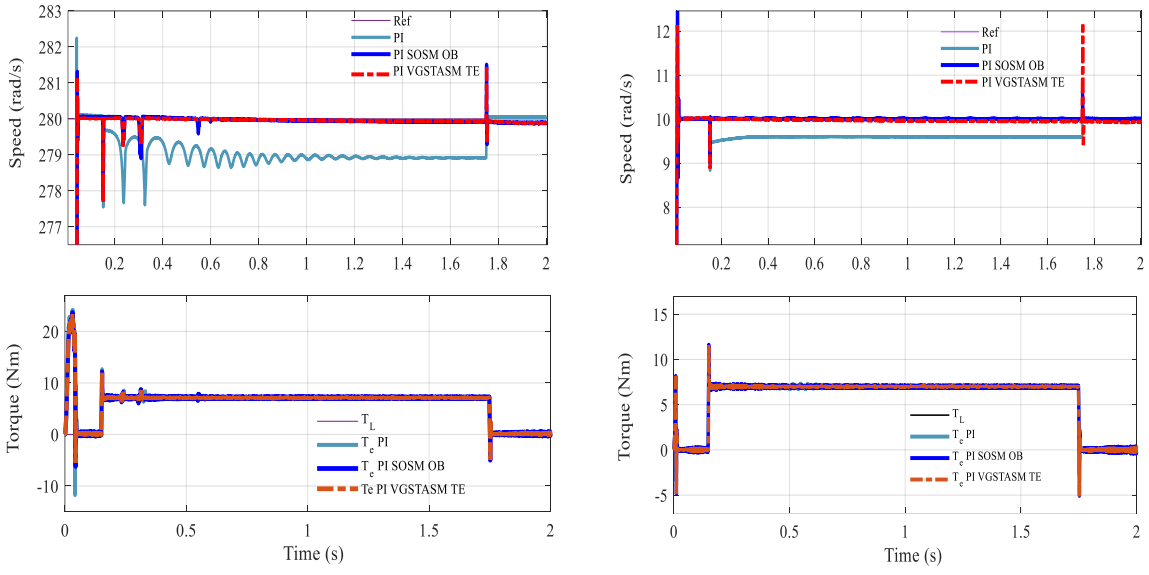

Figure 5. Speed response under Rr variation: (a) speed and torque response at high speed 280rad/s and (b) speed and torque response at low speed 10 rad/s

3.2.2. Influence of inertia variation

A second robustness test was carried out to assess the effect of doubling the total inertia J, which directly affects the mechanical time constant J/B. As seen in Figures 6(a) and (b), the classical PI controller exhibits a slower response and larger overshoot, revealing its poor adaptability to mechanical uncertainties. The PI–SOSM OB achieves better control, yet still suffers from torque ripples and minor steady-state deviations. Meanwhile, the proposed PI–VGSTASM TE maintains both dynamic stability and precise tracking, exhibiting almost identical rise and settling times as in the nominal condition.

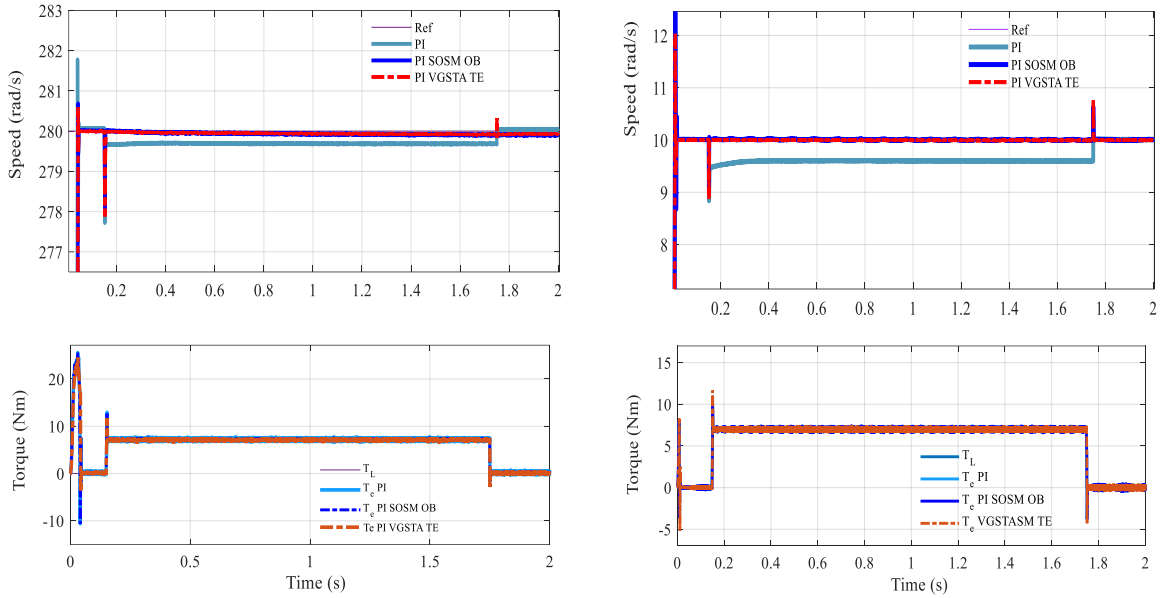

Figure 6. Speed response under J variation: (a) speed and torque response at high speed 280 rad/s and (b) speed and torque response at low speed 10 rad/s

This robustness is mainly due to the VGSTASM-based torque estimation, which actively compensates for inertia-induced disturbances by adjusting the reference isq current in real time. Consequently, both speed and torque remain stable and nearly ripple-free throughout the transient. Overall, the comparative results confirm that the proposed PI–VGSTASM TE strategy provides the highest robustness among the three controllers. It effectively compensates for parameter mismatches in both electrical Rr and mechanical J domains, ensuring accurate tracking, minimal oscillations, and smooth torque dynamics. These features make the approach highly suitable for practical applications requiring consistent performance under uncertain operating conditions.

4. CONCLUSION

This paper has presented a robust and efficient PI_ VGTSTSM TE hybrid control strategy for induction motor drives, targeting applications that demand both high dynamic performance and strong disturbance rejection, such as electric vehicles. The proposed control structure integrates a conventional PI controller for the speed loop, the VGSTASM is employed both for the inner current control loop and for the design of a nonlinear disturbance observer. This design improves the transient response and robustness of the inner loop and disturbance estimator while effectively mitigating chattering. Besides, the gains of the current controller and disturbance observer were optimized by PSO during the design stage to enhance convergence stability and reduce overshoot under parameter variation. The combination of a simple PI controller and advanced nonlinear techniques such as VGSTASM controller allows the system to retain industrial practicality while achieving fast response, high accuracy in speed tracking, and improved robustness against parameter variations and sudden load changes. Simulation results validate that the proposed PI_ VGTSTSM_TE control scheme significantly outperforms conventional PI-based FOC approaches in both transient and steady-state operation, with reduced chattering, improved current regulation, and near-zero steady-state error under variable load conditions. Future research will focus on realizing the proposed

controller in a real-time hardware environment, followed by hardware-in-the-loop (HIL) and laboratory experiments on an induction motor system to verify its practical applicability and robustness in real-world scenarios.

FUNDING INFORMATION

Authors state no funding involved.

AUTHOR CONTRIBUTIONS STATEMENT

This journal uses the Contributor Roles Taxonomy (CRediT) to recognize individual author contributions, reduce authorship disputes, and facilitate collaboration.

Name of Author	C	M	So	Va	Fo	I	R	D	O	E	Vi	Su	P	Fu
Ngoc Thuy Pham	✓	✓	✓	✓	✓		✓	✓	✓	✓		✓	✓	
Duc Thuan Le		✓	✓	✓	✓	✓	✓	✓		✓	✓	✓		
Thanh Tinh Pham		✓	✓		✓	✓	✓		✓				✓	

C : **C**onceptualization
M : **M**ethodology
So : **So**ftware
Va : **Va**lidation
Fo : **Fo**rmal analysis
I : **I**nvestigation
R : **R**esources
D : **D**ata Curation
O : Writing - **O**riginal Draft
E : Writing - Review & **E**diting
Vi : **Vi**sualization
Su : **Su**pervision
P : **P**roject administration
Fu : **Fu**nding acquisition

CONFLICT OF INTEREST STATEMENT

Authors state no conflict of interest.

DATA AVAILABILITY

The data that support the findings of this study are available on request from the corresponding author, [Ngoc Pham]. The data, which contain information that could compromise the privacy of research participants, are not publicly available due to certain restrictions.

REFERENCES

[1] P. Vas, *Sensorless vector and direct torque control*, Oxford University PressOxford, 1998, doi: 10.1093/oso/9780198564652.001.0001.

[2] J. Pyrhöonen, V. Hrabovcová, and S. Semken, *Electrical machine drives control: An introduction*. Wiley, 2016, doi: 10.1002/9781119260479.

[3] G. K. Alitasb, "Integer PI, fractional PI and fractional PI data trained ANFIS speed controllers for indirect field oriented control of induction motor," *Heliyon*, vol. 10, no. 18, Sep. 2024, doi: 10.1016/j.heliyon.2024.e37822.

[4] L. Wogi, T. Ayana, M. Morawiec, and A. Jąderko, "A comparative study of fuzzy SMC with adaptive fuzzy PID for sensorless speed control of six-phase induction motor," *Energies*, vol. 15, no. 21, Nov. 2022, doi: 10.3390/en15218183.

[5] N. T. Pham, "Sensorless speed control of SPIM using BS_PCH novel control structure and NNSM_SC MRAS speed observer," *Journal of Intelligent & Fuzzy Systems*, vol. 39, no. 3, pp. 2657–2677, Oct. 2020, doi: 10.3233/JIFS-190540.

[6] I. Djelamda and I. Bochareb, "Field-oriented control based on adaptive neuro-fuzzy inference system for PMSM dedicated to electric vehicle," *Bulletin of Electrical Engineering and Informatics*, vol. 11, no. 4, pp. 1892–1901, Aug. 2022, doi: 10.11591/eei.v11i4.3818.

[7] N. T. Pham, "An improved BS_NAHOSM hybrid control strategy for FOC of dual Star induction motor drives," *Periodica Polytechnica Electrical Engineering and Computer Science*, vol. 69, no. 3, pp. 226–235, Jul. 2025, doi: 10.3311/PPee.37384.

[8] N. El Ouanjli, A. Derouich, A. El Ghzizal, A. Chebabhi, and M. Taoussi, "A comparative study between FOC and DTC control of the doubly fed induction motor (DFIM)," in *2017 International Conference on Electrical and Information Technologies (ICEIT)*, Nov. 2017, pp. 1–6, doi: 10.1109/EITech.2017.8255302.

[9] K. Rahman *et al.*, "Field-oriented control of five-phase induction motor fed from space vector modulated matrix converter," *IEEE Access*, vol. 10, pp. 17996–18007, 2022, doi: 10.1109/ACCESS.2022.3142014.

[10] I. G. Prieto, M. J. Duran, P. Garcia-Entrambasaguas, and M. Bermudez, "Field-oriented control of multiphase drives with passive fault tolerance," *IEEE Transactions on Industrial Electronics*, vol. 67, no. 9, pp. 7228–7238, Sep. 2020, doi: 10.1109/TIE.2019.2944056.

[11] Y. Xu, B. Zhang, Y. Deng, Y. Kang, X. Liu, and H. Cao, "Robust speed control strategy of PMSMs using improved sliding-mode controller with new reaching law and variable-parameter generalized super-twisting observer," *IEEE Transactions on Power Electronics*, vol. 40, no. 11, pp. 16548–16559, Nov. 2025, doi: 10.1109/TPEL.2025.3592251.

[12] T. G. Workineh, Y. B. Jember, and A. T. Kassie, "Evaluation of intelligent PPI controller for the performance enhancement of speed control of induction motor," *Scientific African*, vol. 22, Nov. 2023, doi: 10.1016/j.sciaf.2023.e01982.

[13] W. Yu, K. Zhu, and Y. Yu, "Variable universe fuzzy PID control for active suspension system with combination of chaotic particle swarm optimization and road recognition," *IEEE Access*, vol. 12, pp. 29113–29125, 2024, doi: 10.1109/ACCESS.2024.3368762.
[14] H. Fadil and M. L. Elhafyani, "Fuzzy-PI controller applied to PMSM speed controller: design and experimental evaluation," *International Journal of Power Electronics*, vol. 11, no. 1, pp. 102–115, 2020, doi: 10.1504/IJPELEC.2020.103952.
[15] J. K. Jain, S. Ghosh, and S. Maity, "Concurrent PI controller design for indirect vector controlled induction motor," *Asian Journal of Control*, vol. 22, no. 1, pp. 130–142, Jan. 2020, doi: 10.1002/asjc.1911.
[16] N. Goel, S. Chacko, and R. N. Patel, "PI controller tuning based on stochastic optimization technique for performance enhancement of DTC induction motor drives," *Journal of The Institution of Engineers (India): Series B*, vol. 101, no. 6, pp. 699–706, Dec. 2020, doi: 10.1007/s40031-020-00496-z.
[17] S. Ustun and M. Demirtas, "Optimal tuning of PI coefficients by using fuzzy-genetic for V/f controlled induction motor," *Expert Systems with Applications*, vol. 34, no. 4, pp. 2714–2720, May 2008, doi: 10.1016/j.eswa.2007.05.029.
[18] N. Mohamad Nordin, N. R. Nik Idris, N. Ahmad Azli, M. Z. Puteh, and T. Sutikno, "Fuzzy-PI torque and flux controllers for DTC with multilevel inverter of induction machines," *International Journal of Power Electronics and Drive Systems (IJPEDS)*, vol. 5, no. 2, pp. 268–282, Oct. 2014, doi: 10.11591/ijpeds.v5i2.6581.
[19] H. Li, B. Song, T. Chen, Y. Xie, and X. Zhou, "Adaptive fuzzy PI controller for permanent magnet synchronous motor drive based on predictive functional control," *Journal of the Franklin Institute*, vol. 358, no. 15, pp. 7333–7364, Oct. 2021, doi: 10.1016/j.jfranklin.2021.07.024.
[20] T. Li, A. Li, and L. Hou, "Improved GOA-based fuzzy PI speed control of PMSM with predictive current regulation," *PLOS ONE*, vol. 20, no. 1, Jan. 2025, doi: 10.1371/journal.pone.0318094.
[21] W. Bu, S. Guo, Z. Fan, and J. Li, "Improved adaptive PI-like fuzzy control strategy of permanent magnet synchronous motor," *Energies*, vol. 18, no. 2, Jan. 2025, doi: 10.3390/en18020362.
[22] X.-D. Liu, K. Li, and C.-H. Zhang, "Improved backstepping control with nonlinear disturbance observer for the speed control of permanent magnet synchronous motor," *Journal of Electrical Engineering & Technology*, vol. 14, no. 1, pp. 275–285, Jan. 2019, doi: 10.1007/s42835-018-00021-9.
[23] H. Ait Abbas, B. Zegnini, M. Belkheiri, and A. Rabhi, "Radial basis function neural network-based adaptive control of uncertain nonlinear systems," in *2015 3rd International Conference on Control, Engineering & Information Technology (CEIT)*, May 2015, pp. 1–6, doi: 10.1109/CEIT.2015.7233124.
[24] B. Mohapatra, B. K. Sahu, and S. Pati, "A novel optimally tuned super twisting sliding mode controller for active and reactive power control in grid-interfaced photovoltaic system," *IET Energy Systems Integration*, vol. 5, no. 4, pp. 491–511, Dec. 2023, doi: 10.1049/esi2.12117.
[25] X. Xiong, H. Chen, Y. Lou, Z. Liu, S. Kamal, and M. Yamamoto, "Implicit discrete-time adaptive first-order sliding mode control with predefined convergence time," *IEEE Transactions on Circuits and Systems II: Express Briefs*, vol. 68, no. 12, pp. 3562–3566, Dec. 2021, doi: 10.1109/TCSII.2021.3070435.
[26] J. Hong, X. Lin, J. Zhang, W. Huang, B. Yan, and X. Li, "A composite sliding mode control with the first-order differentiator and sliding mode observer for permanent magnet synchronous machine," *ISA Transactions*, vol. 147, pp. 489–500, Apr. 2024, doi: 10.1016/j.isatra.2024.02.006.
[27] P. Proaño, R. Díaz, C. Chillán, J. Medina, W. Chamorro, and J. Zuñiga, "Sliding mode control proposed using a Clegg integrator for speed control of a three-phase induction motor," in *JIEE 2024*, Nov. 2024, p. 8, doi: 10.3390/engproc2024077008.
[28] T. Wang, B. Wang, Y. Yu, and D. Xu, "Discrete sliding-mode-based MRAS for speed-sensorless induction motor drives in the high-speed range," *IEEE Transactions on Power Electronics*, vol. 38, no. 5, pp. 5777–5790, May 2023, doi: 10.1109/TPEL.2023.3236024.
[29] Z. Kang, X. Lin, Z. Liu, X. Shen, Y. Gao, and J. Liu, "Adaptive generalized super-twisting sliding mode control for PMSM drives," *IEEE Transactions on Energy Conversion*, pp. 1–11, 2025, doi: 10.1109/TEC.2025.3590203.
[30] R. Seeber and M. Reichhartinger, "Conditioned super-twisting algorithm for systems with saturated control action," *Automatica*, vol. 116, Jun. 2020, doi: 10.1016/j.automatica.2020.108921.
[31] H. Zhang, P. Ran, and Z. Zhang, "PMSM sensorless control based on super-twisting algorithm sliding mode observer with the IAORLS parameter estimations," *Scientific Reports*, vol. 15, no. 1, Jul. 2025, doi: 10.1038/s41598-025-04030-3.
[32] J. Liu, J. Zhu, K. Khayati, D. Zhong, and J. Jiang, "Exponential super-twisting control for nonlinear systems with unknown polynomial perturbations," *Scientific Reports*, vol. 14, no. 1, Feb. 2024, doi: 10.1038/s41598-024-53761-2.
[33] L. Tan, J. Gao, Y. Luo, and L. Zhang, "Super-twisting sliding mode control with defined boundary layer for chattering reduction of permanent magnet linear synchronous motor," *Journal of Mechanical Science and Technology*, vol. 35, no. 5, pp. 1829–1840, May 2021, doi: 10.1007/s12206-021-0403-9.
[34] A. Karami-Mollaee and O. Barambones, "Higher order sliding mode control of MIMO induction motors: A new adaptive approach," *Mathematics*, vol. 11, no. 21, Nov. 2023, doi: 10.3390/math11214558.
[35] J. A. Moreno, H. Rios, L. Ovalle, and L. Fridman, "Multivariable super-twisting algorithm for systems with uncertain input matrix and perturbations," *IEEE Transactions on Automatic Control*, vol. 67, no. 12, pp. 6716–6722, Dec. 2022, doi: 10.1109/TAC.2021.3130880.
[36] S. Ding, Q. Hou, and H. Wang, "Disturbance-observer-based second-order sliding mode controller for speed control of PMSM drives," *IEEE Transactions on Energy Conversion*, vol. 38, no. 1, pp. 100–110, Mar. 2023, doi: 10.1109/TEC.2022.3188630.
[37] X. Lin, B. Zhang, S. Fang, R. Xu, S. Guo, and J. Liu, "Adaptive generalized super twisting sliding mode control for PMSMs with filtered high-gain observer," *ISA Transactions*, vol. 138, pp. 639–649, Jul. 2023, doi: 10.1016/j.isatra.2023.02.008.
[38] H. Benderradji, S. Benaicha, and L. C. Alaoui, "Improved sliding mode control for induction motor based on twisting algorithm," *AIMS Electronics and Electrical Engineering*, vol. 9, no. 1, pp. 81–98, 2025, doi: 10.3934/electreng.2025005.
[39] T. Wang, B. Wang, Y. Yu, and D. Xu, "Fast high-order terminal sliding-mode current controller for disturbance compensation and rapid convergence in induction motor drives," *IEEE Transactions on Power Electronics*, vol. 38, no. 8, pp. 9593–9605, Aug. 2023, doi: 10.1109/TPEL.2023.3277886.
[40] D. Zhang, J. Hu, J. Cheng, Z.-G. Wu, and H. Yan, "A novel disturbance observer based fixed-time sliding mode control for robotic manipulators with global fast convergence," *IEEE/CAA Journal of Automatica Sinica*, vol. 11, no. 3, pp. 661–672, Mar. 2024, doi: 10.1109/JAS.2023.123948.
[41] K. Guo, C. Wei, and P. Shi, "Fuzzy disturbance observer-based adaptive nonsingular terminal sliding mode control for multi-joint robotic manipulators," *Processes*, vol. 13, no. 6, May 2025, doi: 10.3390/pr13061667.
[42] Y. Deng, J. Zhu, and H. Liu, "The improved particle swarm optimization method: An efficient parameter tuning method with the tuning parameters of a dual-motor active disturbance rejection controller," *Sensors*, vol. 23, no. 20, Oct. 2023, doi: 10.3390/s23208605.

[43] J. Shi, Q. Mi, W. Cao, and L. Zhou, "Optimizing BLDC motor drive performance using particle swarm algorithm-tuned fuzzy logic controller," *SN Applied Sciences*, vol. 4, no. 11, Nov. 2022, doi: 10.1007/s42452-022-05179-6.
[44] N. Derbel, J. Ghommam, and Q. Zhu, *Applications of sliding mode control*, vol. 79. Singapore: Springer Singapore, 2017, doi: 10.1007/978-981-10-2374-3.
[45] Y. Shtessel, C. Edwards, L. Fridman, and A. Levant, *Sliding mode control and observation*. New York, NY: Springer New York, 2014, doi: 10.1007/978-0-8176-4893-0.

BIOGRAPHIES OF AUTHORS

Ngoc Thuy Pham is a lecturer in Department of Electrical Engineering Technology, Industrial University of Ho Chi Minh City (IUH), Ho Chi Minh, Viet Nam. She received the B.Sc. and M.Sc. degrees in Electrical Engineering from Thai Nguyen University of Technology in 1994 and Ho Chi Minh City University of Technology (HCMUT) in 2009, respectively. and Ph.D. degree in Control Engineering and Automation from TE and Electrical Engineering from Ho Chi Minh City University of Transport, in 2020. Her current research interests include power electronics, AC motor drives, intelligent control, multiphase induction motor, sensorless control of multiphase induction motor drives, embedded system. She can be contacted at email: phamthuyngoc@iuh.edu.vn.

Duc Thuan Le is a lecturer in Department of Electrical Engineering Technology, Industrial University of Ho Chi Minh City (IUH), Ho Chi Minh, Viet Nam. He received the B.Sc. degree in Electrical Engineering from Thai Nguyen University of Technology in 1994, and M.Sc. degree in Control Engineering and Automation from Ha Noi University of Transport, in 2020. His research interests include the field of power electronics, intelligent control, multiphase induction motor, AC motor drives, embedded system. He can be contacted at email: leducthuan@iuh.edu.vn.

Thanh Tinh Pham was born in 2000, in Vietnam. He received his Engineer's degree in Electrical and Electronic Engineering from Ho Chi Minh City University of Industry in 2022. In 2023, he began pursuing the Master's program at Ho Chi Minh City University of Industry. His research interests include motor drives, multiphase motors, renewable energy, embedded systems, and intelligent control. He can be contacted at email: 22734111.tinh@student.iuh.edu.vn.